

CHALMERS



Finding the Jeffrey Orbits

Master's Thesis in Complex Adaptive Systems

Staffan Ankardal

Department of Physics & Engineering Physics
Non-linear Dynamics & Statistical Physics
CHALMERS UNIVERSITY OF TECHNOLOGY
Gothenburg, Sweden 2011
Master's Thesis 2011:1

Abstract

The Jeffrey orbits define the motion of axissymmetrical particles in shear flow and is thus important in the study of suspensions of particles. In these theses we verify the equations of motion experimentally using glass particles in a reversible flow in a PDMS microchannel and an optical tweezer. We also study the effects of asymmetry on the particles and study the transition from periodic to quasi-periodic orbits for different initial conditions and degrees of asymmetry. A good match with theoretical results are found, but there are some unexplained behaviours when the flow is reversed.

Acknowledgements

I hereby wish to thank my girlfriend Callie Gibbons for supporting me through the work on this thesis and Alexander Laas for being a tireless and understanding co-worker. I want to thank my supervisors Bernhard Mehlig and Dag Hanstorp for helping with good suggestions. I want to thank all the contributors to the wealth of open source software which I have used to create everything from most of the software to more of the figures and of course this very report.

Staffan Ankardal, Göteborg Sweden INSERT PROPER DATE 3/11/13

Contents

1	Introduction	1
1.1	Introduction	1
1.1.1	Background	1
2	Theory	3
2.1	Fluid Dynamics	3
2.1.1	Navier Stokes	3
2.1.2	Reynold's Number	3
2.1.3	Stokes Drag and Stokes's law	4
2.1.4	Shear	5
2.1.5	Péclet Number	5
2.2	Euler Angles and our Coordinate System	5
2.3	Jeffrey Orbits	5
2.3.1	Winding Number	8
2.4	Kalman filter	8
3	Method	9
I	Improvements of Experimental Setup	10
3.1	Improvements	11
3.1.1	Particles and Channel	11
3.1.2	Automated Tracking	14
3.2	Experimental Setup	14
3.2.1	Density matching	16
3.3	Particle tracking	17
3.3.1	Noise Reduction	17
3.3.2	Canny Edge Detection	17
3.3.3	Contour detection and selection	17
3.3.4	Stabilizing the tracking	18
3.3.5	Time Considerations	18

3.4	Kalman Filter	19
3.5	Data Analysis	20
3.5.1	Particle identification	20
3.5.2	Estimation of orientation	21
3.5.3	Width compensation	22
3.5.4	brushing	22
4	Results	23
5	Discussion	24
A	Raw data	25

1

Introduction

1.1 Introduction

The goal of this thesis is to study and better understand the dynamics of ellipsoidal particles in shear flow, and is a continuation of two previous masters theses [1, 2]. This is done by analysing micrometer length glass particles in a shear flow and comparing this to theoretical models. Before discussing either of these processes more in depth some background and basic theory is needed.

1.1.1 Background

The study of particle dynamics in flow began with Einstein's paper from 1905 [3] in which he showed that the viscosity of suspended particles would increase the viscosity of the fluid and by how much. Jeffrey in his 1922 paper [4] extended these results to ellipsoidal axis-symmetrical particles as well as derived equations for the orientational dynamics of the particles. For systems where inertial effects could be discarded the motion was found to be periodic and depending only on the initial condition of the particle.

Developments on triaxial particles, started with Gierszewski & Chaffey (1978)[5] and was continued by Hinch & Leal (1979)[6] and more recently by Yarin et al in 1993[7]. The dynamics found for axis-symmetric particles by Jeffrey were periodic, but it was shown by Hinch & Leal that some orbits would be doubly periodic, in other words following two separate independent periods. Yarin then was able to use numerical simulations to generate a surface of section [8] for some asymmetric relations between the two minor axes showing that not only was there double periodic or quasi periodic orbits but for sufficiently large asymmetries in axes there would be chaotic orbits. Several other surfaces of were also produced by Johansson (2012)[1] using the same method as Yarin with higher resolution thanks to improvements in computing power. It was there shown that only very small asymmetries on the order of 1% will lead to quasi-periodic motion for some initial conditions.

Experimental studies of these theoretical results were first done by Goldsmith and Mason in 1962[9] who confirmed that the rotation rate matched well with that predicted from Jeffrey orbits but he did not study the actual orbits. Since then most experimental research, such as CITE SOME-

1.1. INTRODUCTION

THING HERE has been focused on diluted suspensions of particles and the increased viscocity and other properties this causes. As good summary of both theoretical but primarily experimental results was written by Petrie in 1999 [10].

The first experimental work to try to measure the actual Jeffrey orbits in their Euler angles was done by Einarsson et al [11] in 2011. Although there was some promising results, the vast majority of particles were asymmetric to the point of chaotic or highly quasi-periodic. Moreover the width and length of particles both varied great and could not be measured with good accuracy, meaning that the aspect ratio could not accurately be determined.

2

Theory

In order to better understand the results and discussions in this thesis some rather basic results in fluid dynamics, image analysis and other fields need to be understood by the reader.

- 1) It is however not the focus of this thesis and as such I will try to be as brief as possible, and an experienced reader can safely skip to the next chapter.
- 2) As the focus of this thesis is experimental I will not go into great detail, but try to briefly motivate and quickly summarize results, and refer the inquisitive reader to more thorough sources. As no recent developments are discussed, readers comfortable in these fields can skip this chapter without any loss in understanding.

2.1 Fluid Dynamics

In order to understand the motivations, limitations and behaviour of the experiment we need to know about a few key concepts in fluid dynamics.

2.1.1 Navier Stokes

2.1.2 Reynold's Number

The Reynolds number (Re) is a dimensionless number describing the ratio of inertial forces to viscous forces in a flow. This is not a very strict definition, but suffices to explain that the Reynolds number can be used to characterize the so called flow regime of a system.

The two major flow regimes are Laminar flow, where viscous forces dominate over inertial forces, and the turbulent regime where inertial forces dominate. The area where neither is significantly larger is referred to as transitional flow, which may show either chaotic or laminar behaviour.

A rough characterization of laminar and chaotic flow can be seen in figure 2.1

The Reynolds number (Re) is defined as [12]

$$Re = \frac{UL\rho}{\mu} \quad (2.1)$$

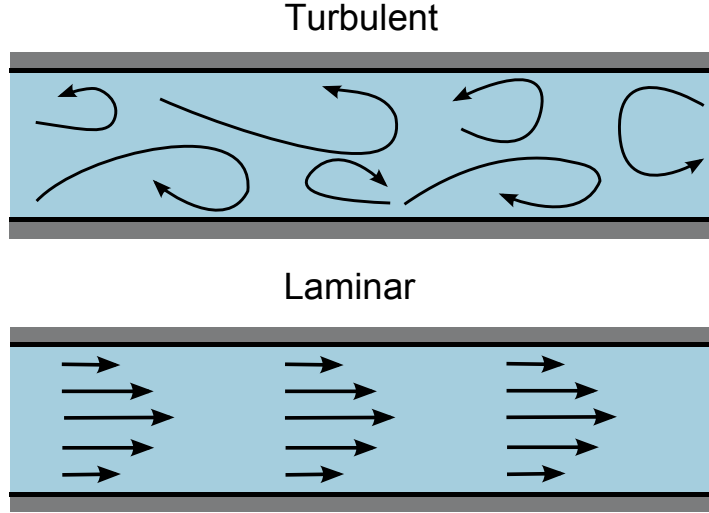


Figure 2.1: This shows the principal difference between laminar and turbulent flow

where U is the characteristic velocity, L is the characteristic length, ρ is the density and μ is the dynamic viscosity.

As the Reynolds number is a ratio, a flow is predicted to be laminar if $Re \ll 1$ which is the primary concern in this thesis.

2.1.3 Stokes Drag and Stokes's law

The drag force exerted by a fluid on a spherical particle for $Re \ll 1$ is found using the so called Stokes's law [13]

$$F_D = 6\pi\mu Rv \quad (2.2)$$

and equating this with the gravitational force acting on the sphere

$$F_G = (\rho_p - \rho_{fl})g \cdot \frac{4\pi R^3}{3} \quad (2.3)$$

the velocity of a steadily sinking sphere is found to be

$$v_s = \frac{2}{9} \frac{\Delta\rho}{\mu} g R^2 \quad (2.4)$$

In order to approximate the falling velocity of our particles we can make use of Stokes law which describes the drag force on an object in laminar flow, and more specifically in the case of a sphere, where $\Delta\rho$ is the difference in density between the sphere and the liquid, g is the specific gravity, μ is the dynamic viscosity and R is the radius of the sphere.

2.1.4 Shear

2.1.5 Péclet Number

The p'clet number describes the ratio of thermal noise to other stuff. I really don't know anything about the piclet number.

2.2 Euler Angles and our Coordinate System

When describing rotating particles it is common to use the so called Euler Angles. A formal definition can be found at MathWorld [14] but for the purposes of this thesis we will describe it as a transformation from a coordinate system $\{x,y,z\}$ to $\{x',y',z'\}$ in three steps

- Rotate the x-y plane ϕ about the z-axis.
- Denote the shifted x axis T and rotate the z-y' plane θ around this axis
- Rotate ψ around the z' axis to obtain the final coordinate system

This is illustrated in figure 2.2 where each prim marks one more step of rotation to the coordinate system. To make it clear how this relates to the experiment figure 2.3 shows the euler angle rotations for a triaxial particle shown from a point of view similar to the of the experiment where the X-Z plane is the primary plane.

2.3 Jeffrey Orbits

The equations of motion for a triaxial ellipsoid particle was first found by Jeffrey [4] but the first dimensionless equation for the Euler Angles was found by Yarin et al. [7] to be

$$\frac{d\theta}{dt} = (g_2 \sin \psi + g_3 \cos \psi) \sin \theta \quad (2.5a)$$

$$\frac{d\phi}{dt} = \frac{1}{2} + g_3 \sin \psi - g_2 \cos \psi \quad (2.5b)$$

$$\frac{d\psi}{dt} = g_1 + (g_2 \cos \psi - g_3 \sin \psi) \cos \theta \quad (2.5c)$$

$$(2.5d)$$

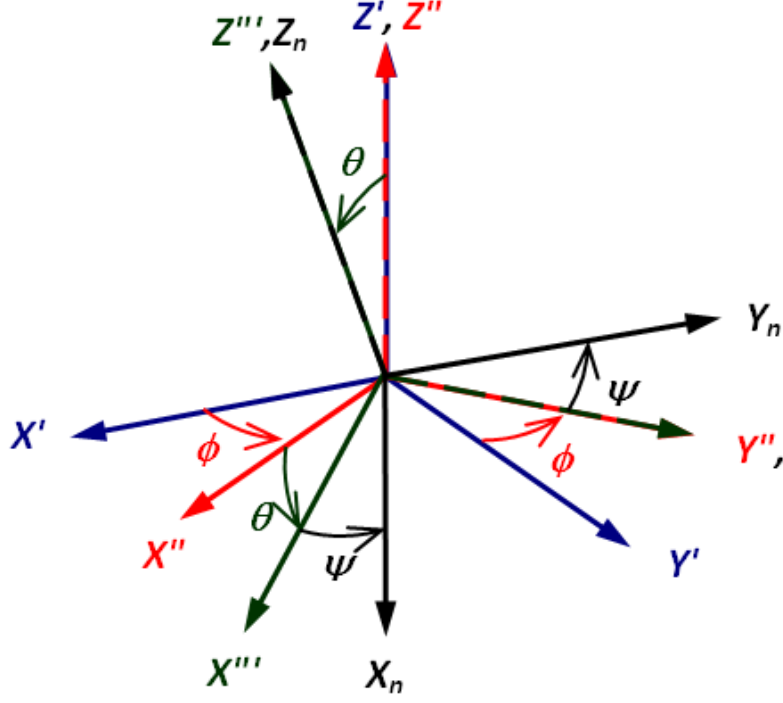


Figure 2.2: The Euler angles illustrated using a series of coordinate rotations. This is the normal way of illustrating the Euler angles as it is how they are defined.

where the functions g_i are defined as

$$g_1 = \frac{a_y^2 - a_z^2}{2(a_y^2 + a_z^2)} \left(-\frac{1}{2}(\cos^2 \theta + 1) \sin 2\phi \sin 2\psi + \cos \theta \cos 2\phi \cos 2\psi \right), \quad (2.6a)$$

$$g_2 = \frac{a_z^2 - a_x^2}{2(a_x^2 + a_z^2)} \left(-\cos \theta \sin 2\phi \sin \psi + \cos 2\phi \cos \psi \right), \quad (2.6b)$$

$$g_3 = \frac{a_x^2 - a_y^2}{2(a_x^2 + a_y^2)} \left(\cos \theta \sin 2\phi \cos \psi + \cos 2\phi \sin \psi \right) \quad (2.6c)$$

where the angles are defined as can be seen in figure 2.2. It should be noted that the Jeffrey orbits sometimes refer simply to solution for the symmetric case (as found by Jeffrey) but this leaves the asymmetric orbits unnamed, so in this thesis Jeffrey Orbits refer to the solutions for both symmetric and asymmetric particles.

The orbits for different initial conditions can be plotted in a Poincaré map [15] for $\phi = 0$. A few such maps can be seen in figure ???. A simplified explanation of the Poincaré map is that a particle starting on some point on a line in the map will follow along that line the next time it intersects with the section, in our case when the particle has $\phi = 0$.

For a particle with a small asymmetry there are essentially three classes of orbits.

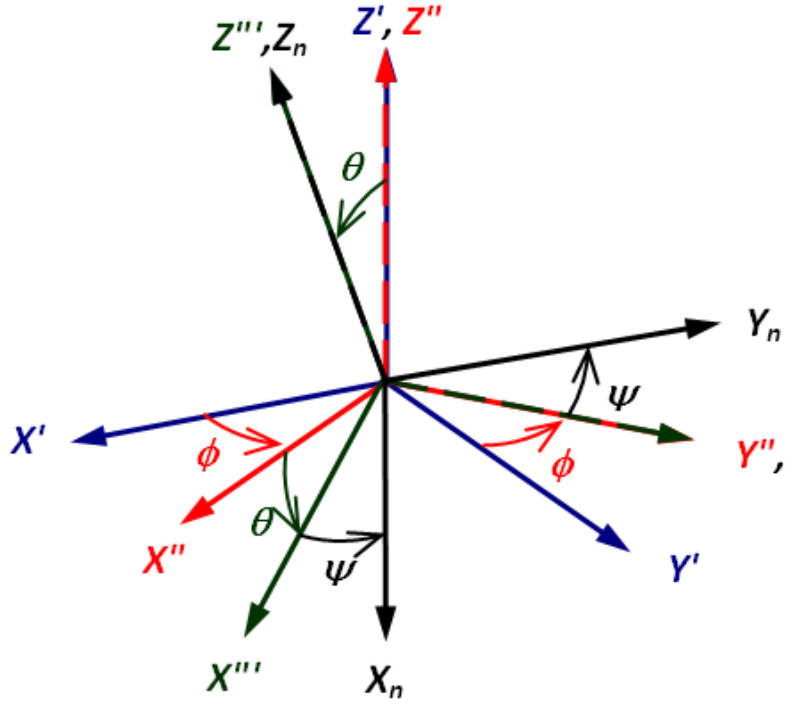


Figure 2.3: The Euler angles illustrated using an ellipsoid. This alternate visualization shows the angles with a point of view similar to that of the camera in the experiment. Note although ψ has an impact on the particle dynamics, as the particle is nearly axis-symmetric we can not observe it

1. Periodic. For larger $|\theta|$ there is little variation and the particle is largely periodic with fluctuations too small to measure.
2. Quasi-periodic bent: For intermediate $|\theta|$ the amplitude of $\cos(\theta)$ changes noticeably but does not change sign.
3. Quasi-periodic circular: For small $|\theta|$ the amplitude of $\cos(\theta)$ will change noticeably and change sign from positive to negative.

These three different types of orbits are illustrated in 2.4 and also shows .

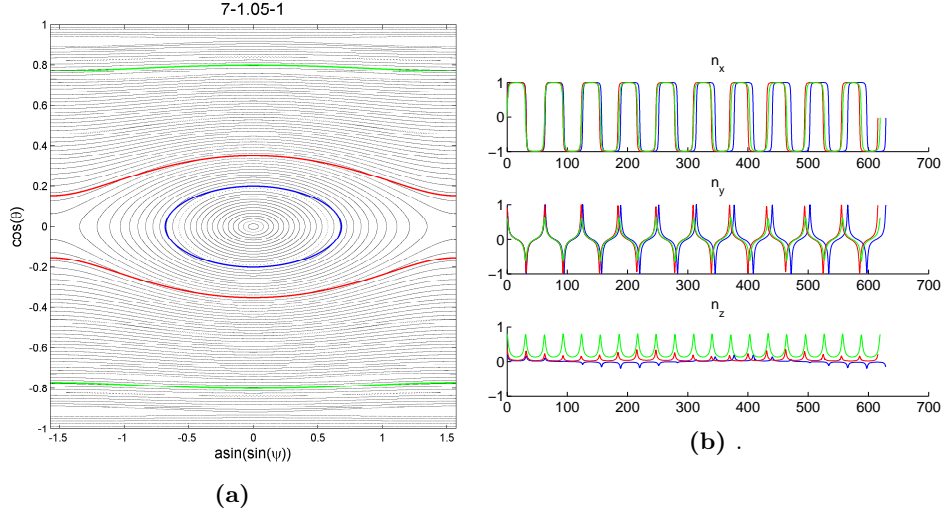


Figure 2.4: .

2.3.1 Winding Number

The quasi-periodic orbits are also referred to as double-periodic. This is referring to the fact that the variations that are seen in figure 2.4b are periodic as well. The ratio between the two periods is referred to as the winding number ω , or simply

$$\omega = \frac{\theta_1}{\theta_2}. \quad (2.7)$$

This can also be thought of as the number of steps travelled on the poincaré map before coming back to where it started, divided by the number of laps it takes. This number is the same for any point along a given orbit on the poincaré map but varies greatly for different orbits as well as for different asymmetries. The winding numbers for orbits a slice along $\psi = 0$ for $\epsilon = \{0.01, 0.05, 0.10\}$ can be seen in figure

2.4 Kalman filter

3

Method

Part I

Improvements of Experimental Setup

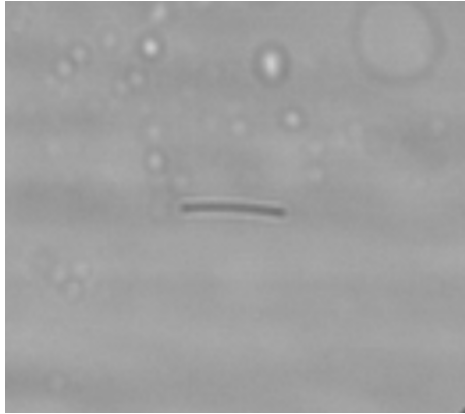
3.1. IMPROVEMENTS

As previously mentioned this thesis is a continuation of work done by Mehlig, Einarsson and Mishra et al [1, 11]. Their results were promising but there were a number of key limitations and problem that we want to solve to improve the results and the ease of getting results. Roughly they are

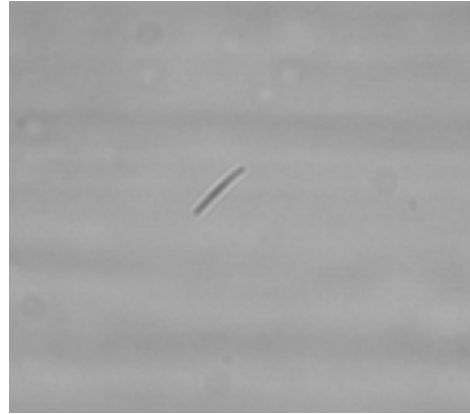
1. The particles
 - Very few particles are symmetric, most are visibly bent or uneven, see figure 3.1
 - Few particles have a low enough aspect to be useful.
 - Have greatly varying and difficult to measure width meaning the aspect ratio cannot be estimated well
 - Cannot be trapped with an optical tweezer due to low transmittance
2. The PDMS in the channel is very jagged which causes a great deal of noise unless the focus is in a very narrow band
3. Manual tracking of particles is time consuming and mentally draining.
4. Bubbles are difficult to avoid when setting up the experiment

3.1 Improvements

3.1.1 Particles and Channel



(a) Particle 13 from July 2012



(b) Particle 22 from July 2012

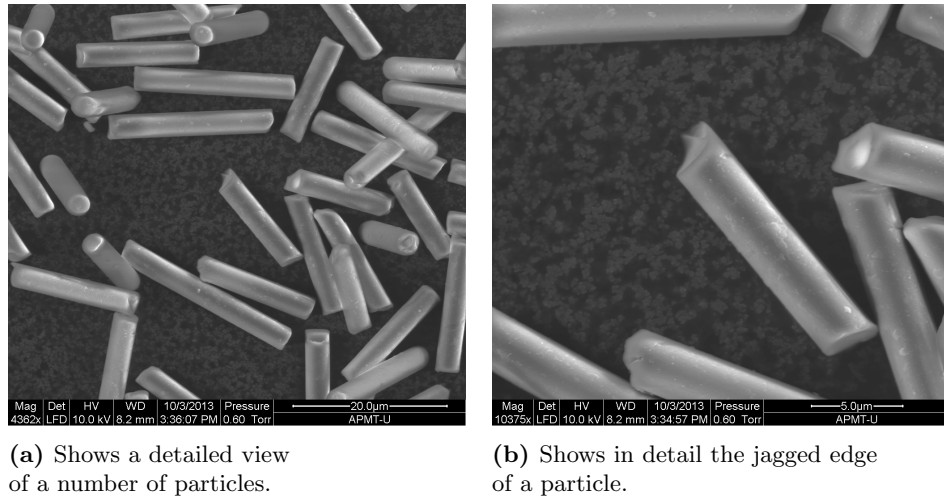
Figure 3.1: Two fairly typical particles from the previous setup. Note that these are still selected from the total pool of particles for being relatively symmetric and yet are noticeably bent.

To solve the problems with the particles we replaced them with glass particles from Nippon Glass, Japan [16]. The particles are made from LCD spacing rods that are , which means they are essentially broken cylinders with very consistent width but quite varying length. Two different batches of particles have been used, one with $3\mu m$ diameter and one batch with $5\mu m$ diameter. All

3.1. IMPROVEMENTS

the particles presented in the results section are from the $3\mu\text{m}$ batch. To verify that the particle were indeed as symmetric and with as even width as we suspected images were taken with an ESEM (Environmental Scanning Electron Microscope) and can be seen in figure 3.2. We see that the particles are uniformly smooth along the edges but have varyingly jagged edges causing different degrees of asymmetry.

In particular figure 3.3b shows a top down view of a particle clearly showing a very circular shape with no discernible asymmetry.



(a) Shows a detailed view of a number of particles.

(b) Shows in detail the jagged edge of a particle.

Figure 3.2: Pictures of the glass particles that particles

3.1. IMPROVEMENTS

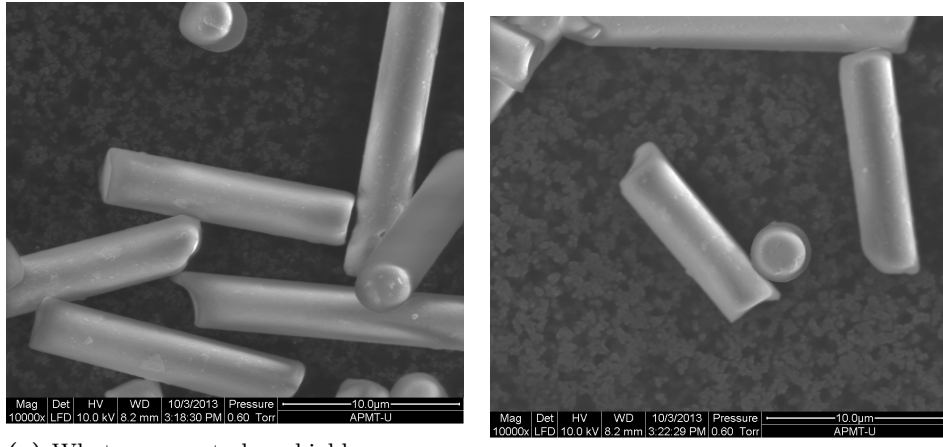
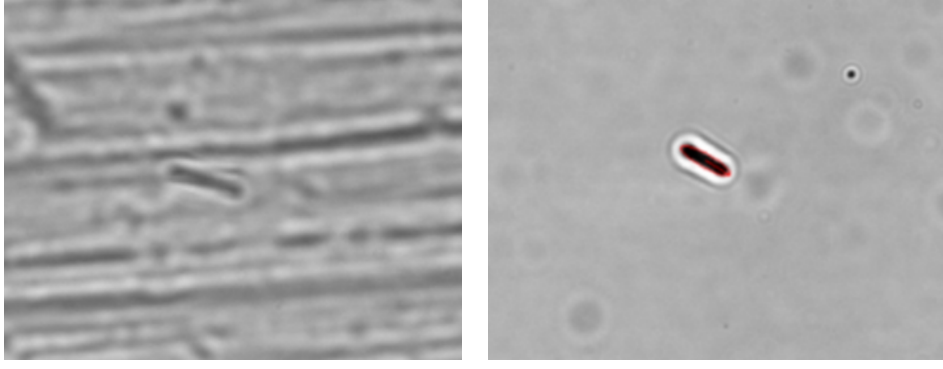


Figure 3.3: Pictures highlighting the roundness of the particles as well as the apparent symmetry of some particles. It should be noted that although there are no apparent rough edges there was no way to rotate a sample so there might very well be asymmetries on the side of the particle that we cannot see.

While these particles seemingly satisfy the symmetry conditions they are made glass with a density of approximately 2.57 g/cm^3 at 20°C which is significantly higher than that of water with a density of 1 g/cm^3 at 20°C and glycerol with a density of 1.5 g/cm^3 . Thus to correct for the density and limit sinking or floating the water soluble Sodium metatungstate which at 20°C has maximum density of 2.94 g/cm^3 . To increase the viscosity of the liquid around 8% glycerol is added, resulting in a measured dynamic viscosity of $24 \cdot 10^{-3} \text{ Pa s}$

A problem in finding and tracking a particle was that the surface of the PDMS was very uneven and one could see sharp ridges along the length of the channel like in figure 3.4a unless the focus was in a relatively narrow depth of the channel.

3.2. EXPERIMENTAL SETUP



(a) An unusual severe case of the PDMS edges creating noise. (b) After being polished there is no trace of such ridges.

Figure 3.4: Pictures highlighting the roundness of the particles as well as the apparent symmetry of some particles. It should be noted that although there are no apparent rough edges there was no way to rotate a sample so there might very well be asymmetries on the side of the particle that we cannot see.

This was fixed by polishing the copper mold in which the PDMS channels are formed with a silicate abbrasive (Autosol) and emery cloth. This reduces all visible scratches from the mold and thus from the PDMS and the result can be seen in figure 3.4b.

3.1.2 Automated Tracking

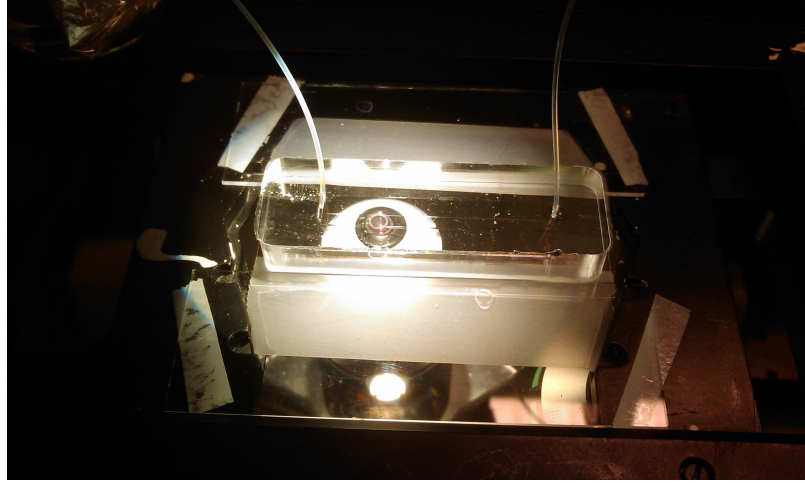
3.2 Experimental Setup

As the goal is to attempt to verify the Jeffrey equations in eq 2.5 we need an experimental setup with particles and flow system that satisfy the conditions that the Jeffrey equations apply under. This means our particles have to be buoyant, triaxially symmetric and small enough that inertial effects are negligible. The flow has to be a linear creeping flow, in other words have a Reynolds number satisfying $Re \ll 1$ and have a high unidirectional shear that allows one to detect the orbits in a relatively short distance.

The particles used in previous measurements were made from epoxy mixed in a vortex[11] which made them buoyant and small enough to ignore inertial effects, but they were not symmetrical enough to produce reliable periodic Jeffrey orbits. Thus two sets of glass particles from Nippon Glass, Japan[16], have been used. They are cylindrical with a consistent width of $3\text{ }\mu\text{m}$ and $5\text{ }\mu\text{m}$ and varying length. Images taken with a STEM microscope can be seen in figure 3.2.

While these particles seemingly satisfy the symmetry conditions they are made glass with a density of approximately 2.57 g/cm^3 at $20\text{ }^\circ\text{C}$ which is significantly higher than that of water with a density of 1 g/cm^3 at $20\text{ }^\circ\text{C}$ and glycerol with a density of 1.5 g/cm^3 . Thus to correct for the density and limit sinking or floating the water soluble Sodium metatungstate which at $20\text{ }^\circ\text{C}$ has maximum density of 2.94 g/cm^3 . To increase the viscosity of the liquid around 8% glycerol is added, resulting in a measured dynamic viscosity of $24 \cdot 10^{-3}\text{ Pa s}$

3.2. EXPERIMENTAL SETUP



This liquid with suspended particles is flowed through a channel of Polydimethylsiloxane (PDMS) 4 cm long, 2.5 mm wide and either 200 μm and 500 μm . The flow profile of such a channel was calculated by Anton Johansson in his thesis[1] and can be seen in figure 3.5. The flow rate varies between 2 and 20 $\mu\text{l}/\text{m}$ or in SI units $3.33 \cdot 10^{-10} \text{ m}^3/\text{s}$ which with a cross section of at least $5 \cdot 10^{-7} \text{ m}^2$ means a maximum flow speed of 6.66 mm/s .

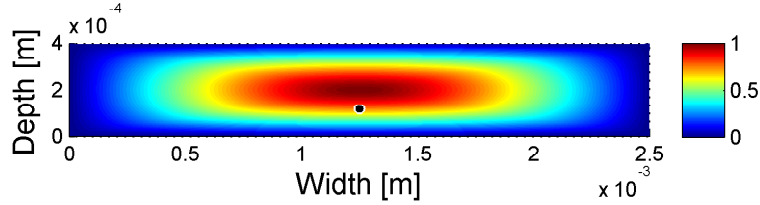


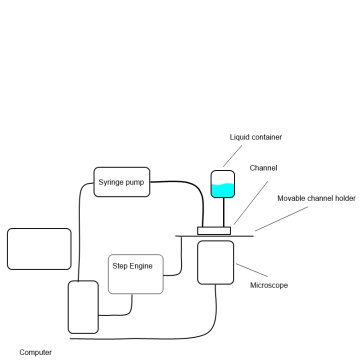
Figure 3.5

To confirm that the flow is a creeping flow we can calculate the maximum Reynolds number using eq 2.1 and our maximum flow speed

$$Re = \frac{UL\rho}{\mu} \leq \frac{6.66 \cdot 10^{-3} \cdot 2.5 \cdot 10^{-3} \cdot 2.5}{24 \cdot 10^{-3}} \approx 1.6 \cdot 10^{-3} \ll 1 \quad (3.1)$$

This should satisfy the conditions of the Jeffrey equations. To track the particles the channel is put in a moveable stage on a confocal microscope. The entire setup can be seen in figure 3.6

3.2. EXPERIMENTAL SETUP



(a) Sketch of the set up



(b) Overview of the set up

Figure 3.6

3.2.1 Density matching

$$\rho_a = \frac{m_a}{V_a} = \frac{V_b \rho_b + V_{mix} \rho_{mix}}{V_b + V_{mix}} \quad (3.2)$$

So if we want to find V_{mix} we get

$$V_{mix} = \frac{V_b(\rho_b - \rho_a)}{\rho_a - \rho_{mix}} \quad (3.3)$$

TODO: READ UP ON THE EFFICIENCY OF THE CANNY EDGE DETECTION TAKE AN IMAGE OF THE STATIC NOISE REDUCTION (DOES IT ACTUALLY WORK?!) GET AN IMAGE OF BEFORE AND AFTER SMOOTHING, PREFERABLY INCLUDE A CANNY EDGE DETECTION OF BOTH WRITE ABOUT THE TIME IT TAKES TO DO VARIOUS STUFFS (IS THIS NEEDED?) GET MORE SOURCES IN THE THEORY SECTION IN PARTICULAR: Looking up reynolds number sources, "creeping motion" might be a relevant term Add our measured visc and add it to citations, maybe add Dag how to cite that?

EULERANGLE STUFF: Find, add and cite a nice definition of the Euler Angles (that I think agree with our definition)

JEFFREY ORBIT STUFF: Make a picture illustrating the various angles Make the poincare map and some n_z/n_x time series and include these mention the aspect ratio and the importance is has

DATA ANALYSIS STUFF: Add citation for Canny edge detection Add citation for ellipse fit Make graph of mode of lengths? Add cite to anton for a bunch of stuff since i am stealing.

EXPERIMENTAL SETUP STUFF: Include the distribution of lengths, either measured or from nippon Make an image of the correction for width and !!!discuss it. !!!

RESULT STUFF

3.3 Particle tracking

3.3.1 Noise Reduction

The first step in tracking a particle is to correctly identify it in the image given. To do this we want to eliminate as much noise from the image as we can. The first type of noise we will eliminate is static noise, this is noise present in every image and results from dirt or scratches on the lens of the camera or microscope. The easiest solution to such noise would of course be to clean the instruments, but despite numerous attempts of carefully cleaning every surface a noticeable of static noise would always remain.

This means one must use algorithmic noise reduction methods to remove this noise. The method employed is a simple averaging that takes N pictures at different positions in the channel to generate an average image where any particular features of the channel would disappear and only the static noise remain. This can be seen in figure STATIC NOISE REDUCTION IMAGE,

3.3.2 Canny Edge Detection

The Canny Edge invented by John Canny in his 2011 paper the canny of cane detection is generally considered the most advanced and best performing edge detection of the simple filter functions. Without going in to the finer details, given an image matrix \mathbf{I} where each value corresponds to the light intensity $i_{x,y}$ of that pixel at index x,y the Canny edge detector will try to find the cohesive pixels $E = \{e_1, e_2 \dots e_n\}$ where there is a noticeable change in intensity. In other words, what we call an "edge" an image.

This is accomplished in two steps. First a Sobel Filter edge image is computed by looking at the change in intensity at every pixel from 3 possible directions and averaging these.

S = MATHEMATICS OF SOBEL

We then consider a Then, a pixel

$p_{x,y} \in E \text{if } S(x,y) > T_{high}$

where T_{high} is a predetermined threshold value.

Secondly we recursively check all pixels neighbouring an edge

MATH?

if they are higher than some threshold value T_{low} . if they are, they are also considered part of the edge. This is repeated until no more pixels are added. An image illustrating this process can be seen in figure FIG. The benefit of the Canny edge detection over the simpler Sobel is that it is much easier to detect cohesive objects that vary in intensity without getting a lot of other noise in the image. The only real drawback of the Canny Edge detection is the computation time, and thus the implementation from the Open Computer Vision (OCV) was used, as this is a heavily optimized routine written in C++ with real time uses in mind. Thanks to this the computing for the Canny Edge of a 260x260 Image takes about X ms and thus is of little importance in the overall time per frame.

After noise reduction the Canny Edge Detection is used to find the most significant edges in the image.

3.3.3 Contour detection and selection

Once an edge image has been generated, the OCV package has another useful function, `Contours` which returns a list of every contiguous group of edge pixels. If we have chosen the threshold values

3.3. PARTICLE TRACKING

to the edge detection correctly, this should include the particle or a good approximation of it.

In order to find the correct contour, a few techniques are used to find the correct contour.

First particles whose total size is less than some minimum value, n_{min} or larger than some maximum value n_{max} are ignored. Then the position pP_i of each contour $C_i = p_1, p_2 \dots p_n$ is calculated as the average pixel position

$$P_i = \sum_j^n p_j / n$$

This position is compared to the expected position of the Kalman filter, which the very first frame is the middle position.

Finally a 'thinness value' is calculated according to eq 3.4

$$w_{thin} \left(\frac{n}{d_{max}^2} \right)^2 \quad (3.4)$$

. where w_{thin} is a weighting constant, n is the number of pixels in the contour and d_{max} is the longest distance between two pixels in the where I am not really sure I should do this now that I have so few particles, but I do it none the less!

3.3.4 Stabilizing the tracking

Once a state estimation has been made, we want to adjust the speed of the step engine to, as best as possible, match that of the particle. This is done by looking both the position and velocity of the particle and going through the conditional statements shown in figure CONDITIONAL CORRECTION VECTOR.

The goal is to limit the amount of corrections made, as changing the velocity is rather time intensive as discussed in section 3.3.5, as well as keeping the particle stable. There is also no point in trying to completely eliminate movement

3.3.5 Time Considerations

A higher FPS will allow the particle detection to be better, improve the position saving and allow the particle tracking to be more stable as well. So maximizing the FPS, ie reducing the computational time of each task, is a clear goal for a good automated tracking. A list of the different tasks and their average execution times can be seen in table 3.1

Task	Average time	Std deviation
Capture screen	1000	200
Find edges	200	20

Table 3.1

We can clearly see that FPS is limited primarily by three routines: The screen capture routine, the change velocity routine and finally the save position routine. The first and last are unavoidable and must be done every frame by definition if we are interested in knowing the particles position as

well as possible. This means we simply want to use the velocity correction as little as possible. Since the time constraint is in the communication with the step engine, there is not any optimization to be done here, at least not within the scope of this thesis.

3.4 Kalman Filter

When the particle is at constant motion in the channel the equations of motion give us

$$\begin{bmatrix} x_n \\ v_{x,n} \\ y_n \\ v_{y,n} \end{bmatrix} = \begin{bmatrix} x_{n-1} & +v_{x,n-1} \\ v_{x,n-1} & \dots \\ y_{n-1} & +v_{y,n-1} \\ v_{y,n-1} \end{bmatrix} + \begin{bmatrix} 0 \\ c_{xn} \\ 0 \\ c_{yn} \end{bmatrix} y_n v_{yn} \quad (3.5)$$

We can rewrite this in matrix form as

$$\begin{bmatrix} x_n \\ v_{x,n} \\ y_n \\ v_{y,n} \end{bmatrix} = \begin{bmatrix} 1 & \Delta t & 0 & 0 \\ 0 & 1 & 0 & 0 \\ 0 & 0 & 1 & \Delta t \\ 0 & 0 & 0 & 1 \end{bmatrix} \cdot \begin{bmatrix} x_{n-1} \\ v_{x,n-1} \\ y_{n-1} \\ v_{y,n-1} \end{bmatrix} + \begin{bmatrix} 0 & 0 & 0 & 0 \\ 0 & 1 & 0 & 0 \\ 0 & 0 & 0 & 0 \\ 0 & 0 & 0 & 1 \end{bmatrix} \cdot \begin{bmatrix} 0 \\ c_{x,n-1} \\ 0 \\ c_{y,n-1} \end{bmatrix} \quad (3.6)$$

Now if we want to transform this to the measured data we have to simply multiply by a constant pixel-to-meter constant, which has been measured to be around $1/940 = 1.06 \cdot 10^{-3}$

$$Q = \begin{bmatrix} 0 & 0 & 0 & 0 \\ 0 & 1 & 0 & 0 \\ 0 & 0 & 0 & 0 \\ 0 & 0 & 0 & 1 \end{bmatrix} \quad (3.7)$$

Which we can easily re-write as a Kalman filter

$$\hat{\mathbf{x}}_n = \mathbf{A}_n \mathbf{x}_{n-1} + \mathbf{B}_n \mathbf{u}_n + \mathbf{w}_n \quad (3.8)$$

$$\hat{\mathbf{P}}_n = \mathbf{F}_n \mathbf{P}_{n-1} \mathbf{F}_n^T + \mathbf{Q}_n \quad (3.9)$$

with

$$\mathbf{x}_n = [x_n v_{x,n} y_n v_{y,n}]^T \quad (3.10)$$

$$\mathbf{A} = \begin{bmatrix} 1 & \Delta t & 0 & 0 \\ 0 & 1 & 0 & 0 \\ 0 & 0 & 1 & \Delta t \\ 0 & 0 & 0 & 1 \end{bmatrix} \quad (3.11)$$

$$\mathbf{B}_n = \begin{bmatrix} 0 & 0 & 0 & 0 \\ 0 & 1 & 0 & 0 \\ 0 & 0 & 0 & 0 \\ 0 & 0 & 0 & 1 \end{bmatrix} \quad (3.12)$$

$$\mathbf{u}_n = \begin{bmatrix} 0 \\ c_{x,n-1} \\ 0 \\ c_{y,n-1} \end{bmatrix} \quad (3.13)$$

and we add the update part as

$$\mathbf{K}_n = \hat{\mathbf{P}}_n \mathbf{H}_n^T (\mathbf{H}_n \hat{\mathbf{P}}_n \mathbf{H}_n^T) \quad (3.14)$$

$$\mathbf{x}_n = \hat{\mathbf{x}}_n + \mathbf{K}_n (\mathbf{y} - \mathbf{H}_n \hat{\mathbf{x}}_n) \quad (3.15)$$

$$\mathbf{P} = (\mathbf{I} - \mathbf{K}_n \mathbf{H}_n) \hat{\mathbf{P}}_n \quad (3.16)$$

3.5 Data Analysis

Once a movie had been recorded we want to estimate the dynamics of the particle. This is done in several steps.

3.5.1 Particle identification

The first step is to reduce the static noise from the movie caused by dirt, scratches and other defects in the microscope and on the camera lens as can be seen in figure 3.7a. As the noise is static and everything else changes this is a simple matter of computing an average frame

$$\bar{F} = \frac{\sum_{n=1}^N F}{den} \quad (3.17)$$

an example of such an average frame can be seen in figure 3.7b. This is then removed from the camera frame and the result can be seen in figure 3.7c. After this we apply a smoothing function and Canny edge detection [?] and then fill the resulting edge. The resulting pixels are then fit to an ellipse as described in [1?]. The filled contour and the fit ellipse can be seen in figure 3.7d.

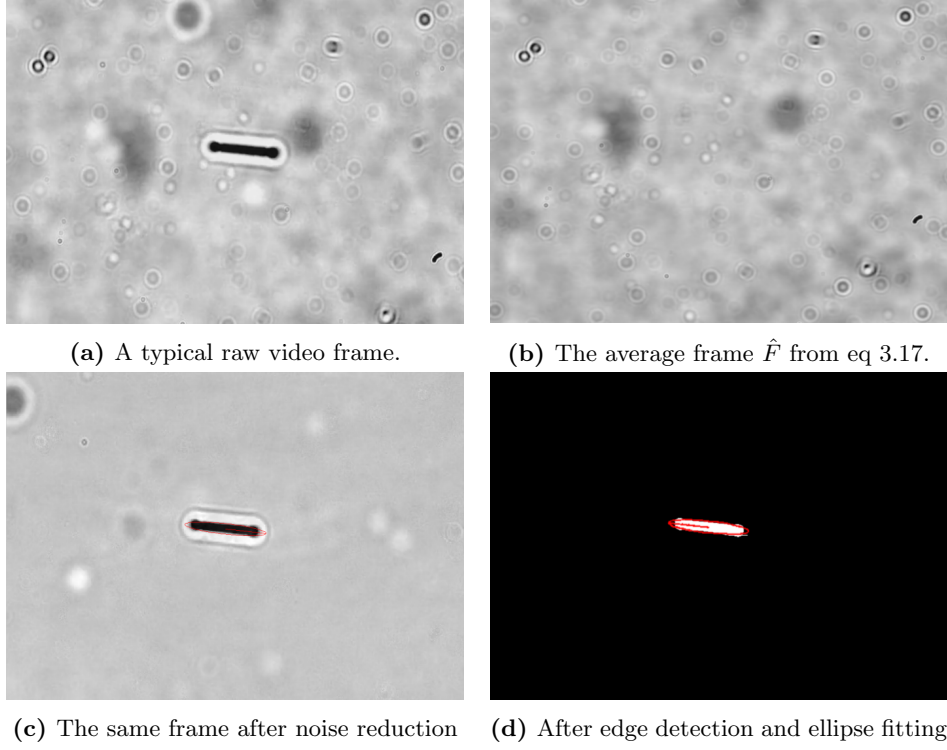


Figure 3.7: These pictures show a simplified version of the image analysis from raw image to estimated particle position

3.5.2 Estimation of orientation

The ellipsoid we get is then our best approximation of the projection of the actual particle. In order to normalize \mathbf{n} we need to know the length of the particle. However as it was shown by Leal that the particle will always spend a majority of its time aligned with the flow, ie aligned with the camera which means that by simply calculating the length L every frame and finding the mode of the distribution we will find a good estimate of L .

So given an ellipsoid with length l_e , width d_e and angle ϕ_p we find

$$p_x = l_e * \sin(\phi_p) \quad (3.18)$$

$$p_z = l_e * \cos(\psi_p) \quad (3.19)$$

with x and z projection p_x and p_z we can get n_x and n_z as well as n_y via

$$n_x = \frac{p_x}{L} \quad (3.20a)$$

$$n_z = \frac{p_z}{L} \quad (3.20b)$$

$$n_y = \sqrt{1 - n_x^2 - n_z^2} \quad (3.20c)$$

3.5.3 Width compensation

Up until this point we have assumed that the particle is a *thin* rod so that the projection \mathbf{p} onto the x and z-axes give us an accurate estimate of \mathbf{n} . However when we are projecting 'thick' particle with length L and width D we get \mathbf{n}' . At $\phi = 0$ this is

$$\mathbf{n}' = n'_z = n_z \cos(\theta) + D \sin(\theta) \quad (3.21)$$

which is illustrated in figure 3.8.

In order to compensate for this error we modify our projection equation 3.18 to

$$p_x = (l_e - w_e) * \sin(\phi_p) \quad (3.22)$$

$$p_z = (l_e - w_e) * \cos(\psi_p) \quad (3.23)$$

This will reduce the particles estimated length by w_e

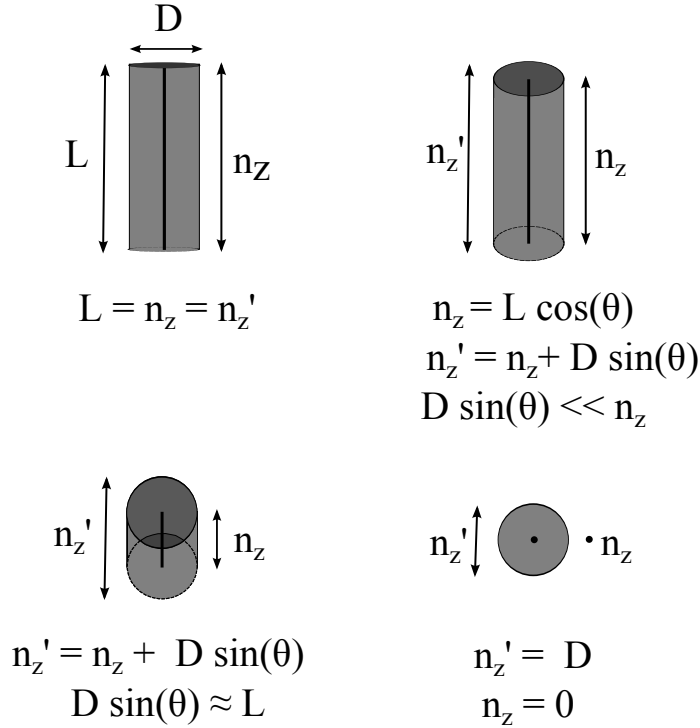


Figure 3.8

3.5.4 brushing

4

Results

The measurements in this section was done together with Alexander Laas.

5

Discussion

A

Raw data

Bibliography

- [1] J. A., Analysis of empirical data on the tumbling of microrods in a shear flow, Master's thesis, Chalmers University of Technology.
- [2] E. J., Low reynolds number particle dynamics, Master's thesis, Chalmers University of Technology.
- [3] A. Einstein, A new determination of molecular dimensions, Annalen der Physik.
- [4] G. B. Jeffrey, The motion of ellipsoidal particles immersed in a viscous fluid, Proceedings of the Royal Society A 102.
- [5] P. J. Gierszewski, C. E. Chaffey, Rotation of an isolated triaxial ellipsoid suspended in slow viscous flow, Canadian Journal of Physics 56 (1) (1978) 6–11.
- [6] L. G. L. E. J. Hinch, Rotation of small non-axissymmetrical particles in a simple shear flow, J. Fluid Mech 92 (1979) 591–608.
- [7] I. V. R. A. L. Yarin, O. Gottlieb, Chaotic rotation of triaxial ellipsoids in simple shear flow, J. Fluid Mech vol 340 (1997) 83–100.
- [8] F. C. van den Bosch, lecture 1: Surfaces of section, Online material for course.
- [9] S. G. M. H. L. Goldsmith, The flow of suspensions through tubes i. single spheres, rods, and discs, Journal of colloid science (17).
- [10] C. J. S. Petrie, The rheology of fiber suspensions, J. of non-newtonian fluid mechanics 87.
- [11] J. E. et al, Periodic and aperiodic tumbling of microrods advected in a microchannel flow, Acta Mechanica (2013) 1–9.
- [12] T. Pedley, Introduction to Fluid Dynamics, Department of Applied Mathematics and Theoretical Physics, University of Cambridge, Silver St., Cambridge CB3 9EW, U.K., 1997.
- [13] G. K. Bachelor, An Introduction to Fluid Dynamics, Cambridge University Press, 1967, page 212 is definition of Reynolds Number, page 233 is Stokes Law.

BIBLIOGRAPHY

- [14] W. E. W, Euler angles, from MathWorld—A Wolfram Web Resource. (2013).
URL <http://mathworld.wolfram.com/EulerAngles.html>
- [15] J. Munkhammar, Poincare map (2013).
URL mathworld.wolfram.com/PoincareMap.html
- [16] N. E. G. Co, Gap spacers for lcds: Microrods, www.neg.co.jp/epd/elm/e_prd/other/others_01.pdf.